Available online at www.sciencedirect.com
SCIENCE DIRECT®
Journal of Solid State Chemistry 174 (2003) 334–341
JOURNAL OF SOLID STATE CHEMISTRY
http://elsevier.com/locate/jssc

Syntheses, structures, optical properties, and theoretical calculations of $Cs_2Bi_2ZnS_5$, $Cs_2Bi_2CdS_5$, and $Cs_2Bi_2MnS_5$

Fu Qiang Huang, Rebecca C. Somers, Adam D. McFarland, Richard P. Van Duyne, and James A Ibers*

Department of Chemistry, Northwestern University, 2145 Sheridan Road, Evanston, IL 60208-3113, USA

Received 24 December 2002; received in revised form 14 April 2003; accepted 25 April 2003

Abstract

Three new compounds, $Cs_2Bi_2ZnS_5$, $Cs_2Bi_2CdS_5$, and $Cs_2Bi_2MnS_5$, have been synthesized from the respective elements and a reactive flux Cs_2S_3 at 973 K. The compounds are isostructural and crystallize in a new structure type in space group *Pnma* of the orthorhombic system with four formula units in cells of dimensions at 153 K of $a=15.763(3)$, $b=4.0965(9)$, $c=18.197(4)$ Å, $V=1175.0(4)$ Å^3 for $Cs_2Bi_2ZnS_5$; $a=15.817(2)$, $b=4.1782(6)$, $c=18.473(3)$ Å, $V=1220.8(3)$ Å^3 for $Cs_2Bi_2CdS_5$; and $a=15.830(2)$, $b=4.1515(5)$, $c=18.372(2)$ Å, $V=1207.4(2)$ Å^3 for $Cs_2Bi_2MnS_5$. The structure is composed of two-dimensional $^2_\infty[Bi_2MS_5^{2-}]$ (M = Zn, Cd, Mn) layers that stack perpendicular to the [100] axis and are separated by Cs^+ cations. The layers consist of edge-sharing $^1_\infty[Bi_2S_6^{6-}]$ and $^1_\infty[MS_3^{4-}]$ chains built from BiS_6 octahedral and MS_4 tetrahedral units. Two crystallographically unique Cs atoms are coordinated to S atoms in octahedral and monocapped trigonal prismatic environments. The structure of $Cs_2Bi_2MS_5$, is related to that of $Na_2ZrCu_2S_4$ and those of the $AMM'Q_3$ materials (A = alkali metal, M = rare-earth or Group 4 element, M' = Group 11 or 12 element, Q = chalcogen). First-principles theoretical calculations indicate that $Cs_2Bi_2ZnS_5$ and $Cs_2Bi_2CdS_5$ are semiconductors with indirect band gaps of 1.85 and 1.75 eV, respectively. The experimental band gap for $Cs_2Bi_2CdS_5$ is $\approx$1.7 eV, as derived from its optical absorption spectrum.

Keywords: Cesium bismuth metal sulfides; Crystal structure; Synthesis; Band gap

1. Introduction

Bismuth oxides and chalcogenides Bi_2Q_3 (Q = S, Se, Te) are of considerable interest owing to their electrical transport properties [1–4]. For example, δ-Bi_2O_3 is one of the best oxide-ion conductors [5,6], and Sb_2Q_3–Bi_2Q_3 mixtures are excellent low-temperature thermoelectric materials [1,7,8]. The formal oxidation state of Bi can be either 3+ or 5+ in oxides, whereas in chalcogenides it is typically 3+ (electronic configuration of $6s^26p^0$ for Bi). The two $6s^2$ valence electrons are stereochemically active and lead to Bi coordination environments of low symmetry. In contrast, the Bi ($6p$) orbitals form bonds with neighboring anions and occupy electronic states near the Fermi level. The important transport properties of Bi chalcogenides arise from these two effects [1,7,8].

Recently, many ternary alkali-metal and alkaline-earth-metal bismuth chalcogenides have been synthesized that also exhibit excellent thermoelectric properties [2,3,9]. The A/Bi/Q (A = alkali metal) and Bi/Cu/Q systems have been studied the most. These include, for example, $CsBiS_2$ [10], $RbBi_3S_5$ [11], $ABiS_2$ (A = Na, K) [12], $K_2Bi_8Se_{13}$ [9,13], Bi_5CuS_8 [14], $BiCu_3S_3$ [15], and $BiCuS_2$ [16]. A number of quaternary bismuth chalcogenides are also known. These include Pb/Bi/Cu/S [17–23] as well as the A/Bi/M/Q phases, with M being primarily Cu, Ag, Si, or Ge. Examples of these are ABi_2CuS_4 (A = K, Cs) [24,25], $RbBi_{2.66}CuSe_5$ [25], $A_3Bi_5Cu_2S_{10}$ (A = K, Rb, Cs) [24,25], $CsBiAg_2S_3$ [25], and $ABiMS_4$ (A = Rb, Cs; M = Si, Ge) [26]. In these compounds, Bi is usually octahedrally coordinated, and less commonly it is coordinated in a 7-octahedron [27], whereas the M atoms are usually tetrahedrally coordinated.

In this present investigation the A/Bi/M/Q systems are extended to include other M atoms with a preference

*Corresponding author. Fax: +1-847-491-2976.
E-mail address: ibers@chem.nwu.edu (J.A. Ibers).

0022-4596/03/$ - see front matter © 2003 Elsevier Inc. All rights reserved.
doi:10.1016/S0022-4596(03)00232-9

for tetrahedral coordination, specifically M = Zn, Cd, Mn. The syntheses, structures, and electronic band structures of $Cs_2Bi_2ZnS_5$, $Cs_2Bi_2CdS_5$, and $Cs_2Bi_2MnS_5$ are reported.

2. Experimental

2.1. Syntheses

The following reagents were used as obtained: Cs (Aldrich, 99.5%), Bi (Johnson Matthey, 99.99%), Zn (Johnson Matthey, 99.99%), Cd (Alfa Aesar, 99.5%), Mn (Alfa Aesar, 99.9%), and S (Alfa Aesar, 99.5%). Cs_2S_3, the reactive flux [28] employed in the syntheses, was prepared by the stoichiometric reaction of the elements in liquid NH_3. Each of the compounds $Cs_2Bi_2MS_5$ (M = Zn, Cd, Mn) was synthesized by the reaction of 1.0 mmol Bi, 0.5 mmol M, 1.0 mmol S, and 0.6 mmol Cs_2S_3. A reaction mixture was loaded into a fused-silica tube under an Ar atmosphere in a glove box. The tube was sealed under a 10^{-4} Torr atmosphere and then placed in a computer-controlled furnace. The sample was heated to 973 K in 12 h, kept at 973 K for 72 h, cooled at 6 K/h to 373 K, and then the furnace was turned off. The reaction mixture was washed with dimethylformamide and then dried with acetone. Each product consisted of black or dark brown needles and some black powder. In each case the yield of needles was approximately 80% based on Bi. Examination of selected needles with an EDX-equipped Hitachi S-3500 SEM led to results consistent with the stated compositions. The compounds are stable in air for a few days.

2.2. Structure determinations

Single-crystal X-ray diffraction data were collected with the use of graphite-monochromatized Mo$K\alpha$ radiation ($\lambda = 0.71073$ Å) at 153 K on a Bruker Smart-1000 CCD diffractometer [29]. The crystal-to-detector distance was 5.023 cm. Crystal decay was monitored by recollecting 50 initial frames at the end of data collection. Data were collected in ω in four groups of 606 frames at φ settings of 0°, 90°, 180° and 270° by a scan of 0.3° for $Cs_2Bi_2ZnS_5$ and $Cs_2Bi_2CdS_5$ with an exposure time of 7 s/frame and by a scan of 0.25° for $Cs_2Bi_2MnS_5$ with an exposure time of 20 s/frame. The collection of the intensity data was carried out with the program SMART [29]. Cell refinement and data reduction were carried out with the use of the program SAINT [29], and face-indexed absorption corrections were performed numerically with the use of the program XPREP [30]. Then the program SADABS [29] was employed to make incident beam and decay corrections.

Each structure was solved with the direct methods program SHELXS and refined with the full-matrix least-squares program SHELXL of the SHELXTL suite of programs [30]. The final refinement included anisotropic displacement parameters and a secondary extinction correction. Additional experimental details are shown in Table 1. Table 2 lists positional parameters and equivalent isotropic displacement parameters and Table 3 presents selected bond distances.

2.3. Optical microspectroscopy measurements

Single-crystal absorption measurements were performed on $Cs_2Bi_2CdS_5$ with the use of an Ocean Optics model S2000 spectrometer over the range 450 nm (2.76 eV) to 1000 nm (1.24 eV) at 293 K. The spectrometer was coupled fiber-optically to a Nikon TE300 inverted microscope. White light originated from a TE300 lamp. The plate-like crystal with dimensions of 5, 20, and 50 μm along [100], [010], and [001], respectively, was mounted along [001] on a glass fiber, and was positioned at the focal point above the 20× objective with the use of a goniometer mounted on translation stages (Line Tool Company). The light transmitted through the crystal was then spatially filtered before being focused into the 400 μm core diameter fiber coupled to the spectrometer. Fine alignment of the microscope assembly was achieved by maximizing the transmission of the lamp profile. The absorption spectrum of light perpendicular to the (100) crystal face was collected.

2.4. TB-LMTO calculations

First-principles self-consistent local density approximation (LDA) [31] calculations of electronic structures on $Cs_2Bi_2ZnS_5$ and $Cs_2Bi_2CdS_5$ were performed with the

Table 1
Crystal data and structure refinements for $Cs_2Bi_2ZnS_5$, $Cs_2Bi_2CdS_5$, and $Cs_2Bi_2MnS_5$

Compound	$Cs_2Bi_2ZnS_5$	$Cs_2Bi_2CdS_5$	$Cs_2Bi_2MnS_5$
Formula weight	909.45	956.48	899.02
Space group	*Pnma*	*Pnma*	*Pnma*
a (Å)	15.763(3)	15.817(2)	15.830(2)
b (Å)	4.0965(9)	4.1782(6)	4.1515(5)
c (Å)	18.197(4)	18.473(3)	18.372(2)
V (Å^3)	1175.0(4)	1220.8(3)	1207.4(2)
Z	4	4	4
T (K)	153(2)	153(2)	153(2)
λ (Å)	0.71073	0.71073	0.71073
ρ_c (g/cm^3)	5.141	5.204	4.946
μ (cm^{-1})	388.35	371.56	368.53
Transm factors	0.015–0.097	0.021–0.241	0.088–0.627
α	0.020	0.030	0.025
$R(F)^a$	0.0238	0.0249	0.0293
$R_w(F_o^2)^b$	0.0526	0.0612	0.0620

[a] $R(F) = \sum ||F_o|-|F_c||/|F_o|$ for $F_o^2 \geq 2\sigma(F_o^2)$.
[b] $R_w(F_o^2) = \sum[w(F_o^2-F_c^2)^2]/\sum wF_o^{4\,1/2}$ for all data. $w^{-1} = \sigma^2(F_o^2) + (\alpha P)^2$ and $P = [2F_c^2 + \max(F_o^2, 0)]/3$.

Table 2
Atomic coordinates[a] and equivalent isotropic displacement parameters for $Cs_2Bi_2ZnS_5$, $Cs_2Bi_2CdS_5$, and $Cs_2Bi_2MnS_5$

Atom	x	z	U_{eq} (Å^2)[b]
$Cs_2Bi_2ZnS_5$			
Cs1	0.00651(3)	0.62205(3)	0.0122(1)
Cs2	0.46014(3)	0.38123(3)	0.0153(1)
Bi1	0.25125(2)	0.01730(2)	0.01126(9)
Bi2	0.29337(2)	0.69783(2)	0.00978(9)
Zn	0.20610(5)	0.35545(5)	0.0092(2)
S1	0.1063(1)	0.2571(1)	0.0103(4)
S2	0.1402(1)	0.4718(1)	0.0096(4)
S3	0.2140(1)	0.8438(1)	0.0117(4)
S4	0.3189(1)	0.1481(1)	0.0100(4)
S5	0.3684(1)	0.5627(1)	0.0120(4)
$Cs_2Bi_2CdS_5$			
Cs1	0.00644(3)	0.62705(3)	0.0157(1)
Cs2	0.46483(3)	0.38778(3)	0.0170(1)
Bi1	0.25564(2)	0.01784(2)	0.0156(1)
Bi2	0.29293(2)	0.69497(2)	0.0132(1)
Cd	0.21184(3)	0.35428(3)	0.0117(1)
S1	0.1050(1)	0.2497(1)	0.0123(4)
S2	0.1355(1)	0.4751(1)	0.0135(4)
S3	0.1998(1)	0.8390(2)	0.0208(5)
S4	0.3183(1)	0.1470(1)	0.0128(4)
S5	0.3635(1)	0.5617(1)	0.0144(4)
$Cs_2Bi_2MnS_5$			
Cs1	0.00771(4)	0.62374(4)	0.0204(2)
Cs2	0.46300(4)	0.38355(4)	0.0242(2)
Bi1	0.25315(2)	0.01740(2)	0.0185(1)
Bi2	0.29325(2)	0.69655(2)	0.0166(1)
Mn	0.20939(9)	0.35439(8)	0.0140(3)
S1	0.1067(2)	0.2548(1)	0.0160(5)
S2	0.1390(2)	0.4724(1)	0.0155(5)
S3	0.2097(2)	0.8430(2)	0.0208(6)
S4	0.3182(2)	0.1482(1)	0.0162(5)
S5	0.3661(2)	0.5621(1)	0.0185(5)

[a] The y coordinate of all atoms is 1/4.
[b] U_{eq} is defined as one third of the trace of the orthogonalized U_{ij} tensor.

Table 3
Selected bond lengths (Å) for $Cs_2Bi_2ZnS_5$, $Cs_2Bi_2CdS_5$, and $Cs_2Bi_2MnS_5$

Bond	$Cs_2Bi_2ZnS_5$	$Cs_2Bi_2CdS_5$	$Cs_2Bi_2MnS_5$
Cs1–S1 × 2	3.492(2)	3.557(2)	3.545(2)
Cs1–S2	3.452(2)	3.471(2)	3.471(2)
Cs1–S2 × 2	3.530(2)	3.601(2)	3.581(2)
Cs1–S4 × 2	3.464(2)	3.491(2)	3.479(2)
Cs2–S1	3.412(2)	3.371(2)	3.411(3)
Cs2–S3 × 2	3.492(2)	3.458(2)	3.512(2)
Cs2–S5 × 2	3.541(2)	3.551(2)	3.553(2)
Cs2–S5	3.604(2)	3.590(2)	3.622(3)
Bi1–S2 × 2	2.794(1)	2.820(1)	2.812(2)
Bi1–S3	3.211(2)	3.420(3)	3.277(3)
Bi1–S4	2.608(2)	2.583(2)	2.615(2)
Bi1–S5 × 2	2.904(1)	2.927(2)	2.923(2)
Bi2–S1 × 2	2.804(1)	2.827(1)	2.822(2)
Bi2–S3	2.936(2)	3.041(3)	2.998(3)
Bi2–S4 × 2	2.853(1)	2.871(1)	2.866(2)
Bi2–S5	2.730(2)	2.704(2)	2.725(3)
M–S1	2.383(2)	2.567(2)	2.448(3)
M–S2	2.358(2)	2.537(2)	2.438(3)
M–S3 × 2	2.414(1)	2.529(1)	2.448(2)

use of the tight binding (TB) linear muffin-tin orbital (LMTO) method in the atomic sphere approximation (ASA), including the combining correction for the neglected integrals over the interstitial region and the neglected partial waves of high quantum number (program TB-LMTO) [32–34]. ($Cs_2Bi_2MnS_5$ has a much more complex band structure owing to the half-occupied 3d orbitals of Mn atoms, so no calculations on this compound were made.) This method splits the crystal space into overlapping Wigner–Seitz atomic spheres whose radii are chosen to fill completely the crystal volume. All k-space integrations were performed with the tetrahedron method [35,36]. The basis sets consisted of the valence orbitals 6s for Cs; the 6s and 6p orbitals for Bi; the 3d, 4s, and 4p orbitals for Zn; the 4d, 5s, and 5p orbitals for Cd; the 3d, 3s and 3p orbitals for S; and the 1s orbitals for empty spheres. The following orbitals were downfolded by the means of Löwdin's technique [37]: 4f, 5d, and 6p for Cs; 5f and 6d for Bi; 4f for Cd; 3d for S; and the $p-d$ states for the empty spheres. The crystal orbital Hamiltonian population (COHP) [38], which is the density of states weighted by the corresponding Hamiltonian matrix element, was calculated to analyze the strength and nature of bonding. Within the Brillouin zone of the cell of $Cs_2Bi_2MS_5$ (M = Zn, Cd), 621 irreducible k points were used. The high-symmetry points are Γ (0, 0, 0), X $(\frac{1}{2},0,0)$, Y $(0,\frac{1}{2},0)$, Z $(0,0,\frac{1}{2})$, R $(\frac{1}{2},\frac{1}{2},\frac{1}{2})$, S $(\frac{1}{2},\frac{1}{2},0)$, T $(0,\frac{1}{2},\frac{1}{2})$, and U $(\frac{1}{2},0,\frac{1}{2})$ in terms of the reciprocal basis vectors [39].

3. Results

3.1. Syntheses

The compounds $Cs_2Bi_2MS_5$ (M = Zn, Cd, Mn) have been synthesized from the elements in a Cs_2S_3 flux at 973 K in approximately 80% yield based on Bi.

Using the same procedure we were unable to synthesize "$Cs_2Bi_2HgS_5$". Perhaps one should not expect this compound to form. As opposed to Zn, Cd, and Mn, Hg has less of a tendency to be tetrahedrally coordinated by four S atoms. Thus, Bi_2HgS_4 [40] and Sb_4HgS_8 [41] contain two- and three-coordinate Hg and many alkali-metal mercury sulfides contain linear HgS_2 units [42–45].

3.2. Structures

The isostructural compounds $Cs_2Bi_2MS_5$ (M = Zn, Cd, Mn) crystallize in a new structure type, as shown in

Fig. 1 for M = Zn. In this structure there is no detectable disorder among Cs, Bi, M, and S atoms. Moreover, there are no S–S bonds in the structure so that formal oxidation states of 1+, 3+, 2+, and 2− may be assigned to Cs, Bi, M, and S, respectively. The structure is composed of two-dimensional $^{2}_{\infty}[Bi_2MS_5^{2-}]$ layers perpendicular to [100] separated by Cs atoms. The two unique Cs atoms (Cs1 and Cs2) in the structure are coordinated to S atoms in an octahedral and a monocapped trigonal prismatic fashion, respectively.

The $^{2}_{\infty}[Bi_2ZnS_5^{2-}]$ layer in $Cs_2Bi_2ZnS_5$ is constructed from BiS_6 octahedra and ZnS_4 tetrahedra (Fig. 2). Each BiS_6 octahedron shares its edges with two others along [010] to form a one-dimensional $^{1}_{\infty}[BiS_4^{5-}]$ chain. Two neighboring $^{1}_{\infty}[BiS_4^{5-}]$ chains link together by edge-sharing to form a $^{1}_{\infty}[Bi_2S_6^{6-}]$ double chain. Each BiS_6 octahedron in the $^{1}_{\infty}[Bi_2S_6^{6-}]$ chain shares a vertex (S3) with another octahedron in a different chain to form a two-dimensional $^{2}_{\infty}[Bi_2S_5^{4-}]$ layer. The ZnS_4 tetrahedron forms a one-dimensional $^{1}_{\infty}[ZnS_3^{4-}]$ chain along [010] by sharing its vertices (S3) with two neighboring tetrahedra. Each ZnS_4 tetrahedron in the $^{1}_{\infty}[ZnS_3^{4-}]$ chain links with four BiS6 octahedra by edge-sharing. These alternating $^{1}_{\infty}[Bi_2S_6^{6-}]$ and $^{1}_{\infty}[ZnS_3^{4-}]$ chains are connected to form the two-dimensional $^{2}_{\infty}[Bi_2ZnS_5^{2-}]$ layer in (100). The succession of polyhedra in this layer is *oct oct tet oct oct tet,* where *oct* = octahedron, tet = tetrahedron.

Each of the two unique Bi atoms (Bi1, Bi2) in these structures is octahedrally coordinated by six S atoms, as shown for $Cs_2Bi_2ZnS_5$ in Fig. 3. These octahedra have crystallographically imposed symmetry m, but are otherwise distorted, especially the Bi1 octahedra (Table 3). Thus the differences between the shortest and the longest Bi1–S bonds are 0.603(3), 0.837(4), and 0.662(4) Å for M = Zn, Cd, and Mn, respectively. Differences of this order are found in other highly distorted BiS_6 octahedra, for example 0.666(1) and 0.71(5) Å in $RbBiMS_4$ (M = Si, Ge) [26] and $HgBi_2S_4$ [40], respectively. These distortions presumably are manifestations of the stereochemically active lone pair of electrons on Bi^{3+} [46].

Each structure contains a unique MS_4 tetrahedron with crystallographically imposed symmetry m. These tetrahedra are minimally distorted, with distances comparable to those in $BaLn_2MS_5$ (Ln = La, Ce, Pr, Nd; M = Zn, Mn) [47] and $Ba_4Ln_2Cd_3S_{10}$ (Ln = Sm, Gd, Tb) [48], respectively.

The $Cs_2Bi_2MS_5$ (M = Zn, Cd, Mn) structure type is closely related to the $KZrCuS_3$, $NaTiCuS_3$, and

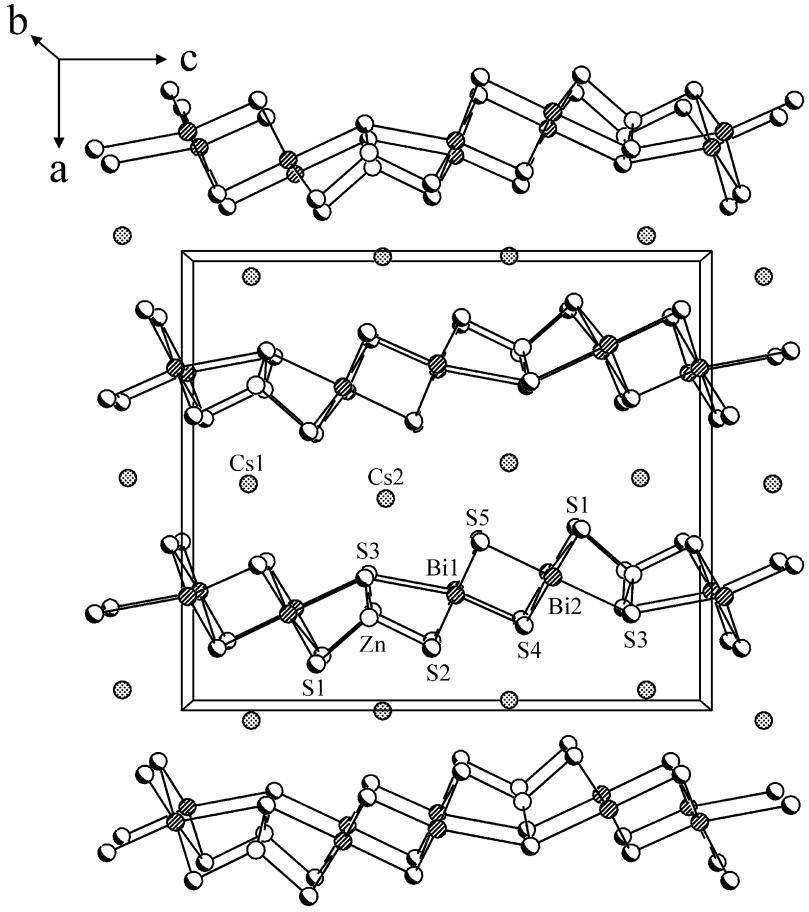

Fig. 1. The unit cell of $Cs_2Bi_2ZnS_5$ along [010].

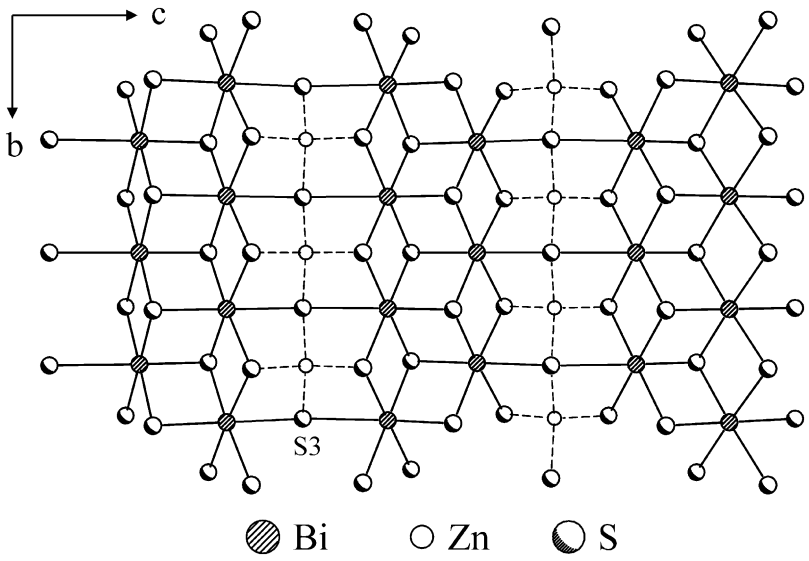

Fig. 2. The $^{2}_{\infty}[Bi_2ZnS_5^{2-}]$ layer in $Cs_2Bi_2ZnS_5$.

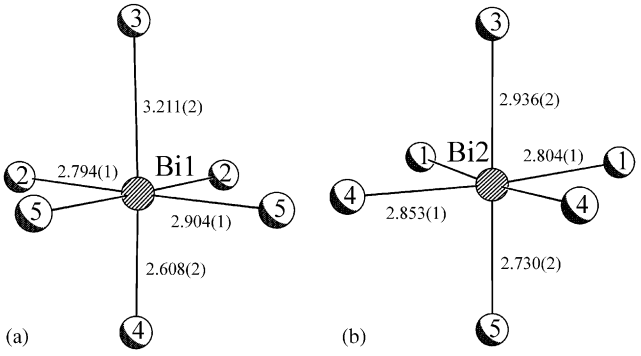

Fig. 3. The coordination environments of (a) Bi1 and (b) Bi2 in $Cs_2Bi_2ZnS_5$.

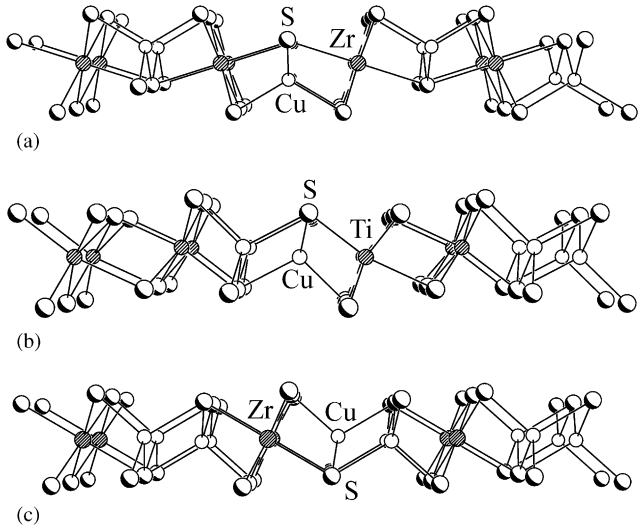

Fig. 4. The layers comprised of octahedra and tetrahedra in (a) $KZrCuS_3$, (b) $NaTiCuS_3$, and (c) $Na_2ZrCu_2S_4$.

$Na_2ZrCu_2S_4$ structure types. Each contains two-dimensional layers of M octahedra (oct) and M' tetrahedra (tet) formed by means of edge- or vertex-sharing, as shown in Fig. 4. These layers are separated by the alkali-metal atoms. The layers in $Cs_2Bi_2ZnS_5$ and $KZrCuS_3$ are similar, except that the $^{2}_{\infty}[ZrCuS_3^{1-}]$ layer in $KZrCuS_3$ consists of a single octahedral $^{1}_{\infty}[ZrS_4^{4-}]$ chain and a single tetrahedral $^{1}_{\infty}[CuS_3^{5-}]$ chain, as shown in Fig. 4. The $^{2}_{\infty}[ZrCuS_3^{-}]$ layer can be labeled in the fashion *oct tet oct tet*. Table 4 and Fig. 4 delineate the ordering of the octahedra and tetrahedra in these various structure types.

One might expect the structure of $Cs_2Bi_2MS_5$ (M = Zn, Cd, Mn) to be closely related to that of $BaLn_2MS_5$ (Ln = La, Ce, Pr, Nd; M = Zn, Mn) [47] because of the similarity in size and coordination preferences of Bi^{3+} versus Ln^{3+}. However, the structure of $BaLn_2MS_5$ is composed of the $^{2}_{\infty}[Ln_2MS_5^{2-}]$ layers, but these are completely different from those in $Cs_2Bi_2MS_5$. In $BaLn_2MS_5$ (space group: $I4/mcm$), each Ln polyhedron is surrounded by four M polyhedra. The Ln and M atoms are coordinated to eight and four S atoms, respectively.

3.3. Optical absorption measurements

The optical absorption spectrum obtained with light perpendicular to the (100) crystal plane for $Cs_2Bi_2CdS_5$ is shown in Fig. 5. The periodic modulation in the spectrum at low energies is an interference pattern caused by the finite thickness of the crystal. This artifact has no influence on the determination of the band gap energy, which is approximately 1.7 eV.

Table 4
Some quaternary alkali-metal chalcogenides with tetrahedral/octahedral layers

Compound	Space group	Ordering of polyhedra	Ref.
$NaZrCuS_3$			[49]
$KZrCuS_3$			[50]
$KZrCuSe_3$	*Cmcm*	*oct tet oct tet*	[50]
$KZrCuTe_3$			[50]
$TlZrCuSe_3$			[49]
$NaTiCuS_3$			[49]
$NaZrCuSe_3$	*Pnma*	*oct oct tet tet oct oct tet tet*	[49]
$NaZrCuTe_3$			[49]
$TlTiCuTe_3$	$P2_1/m$	*oct oct tet tet oct oct tet tet*	[51]
$Na_2ZrCu2S_4$	$C2/m$	*oct tet tet oct tet tet*	[52]
$Cs_2Bi_2ZnS_5$			Current work
$Cs_2Bi_2CdS_5$	*Pnma*	*oct oct tet oct oct tet*	Current work
$Cs_2Bi_2MnS_5$			Current work

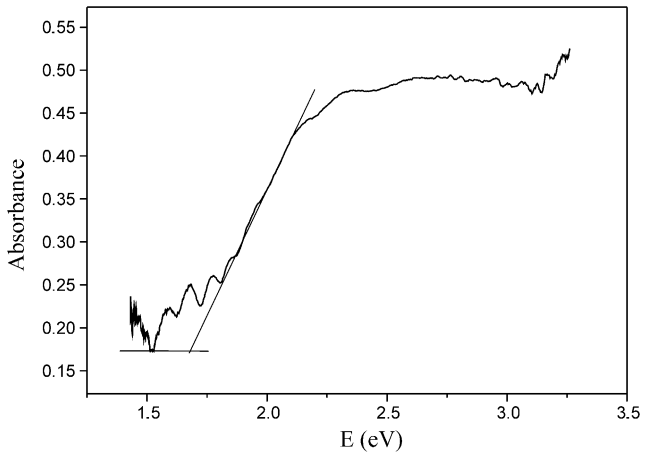

Fig. 5. Optical absorption spectrum of $Cs_2Bi_2CdS_5$.

3.4. Theoretical calculations

First principles density functional theory calculations were performed on $Cs_2Bi_2ZnS_5$ and $Cs_2Bi_2CdS_5$. Their electronic band structures are similar, and only the band structure of $Cs_2Bi_2ZnS_5$ is displayed in Fig. 6. The highest occupied molecular orbitals (HOMO) occur at three non-special k-point positions, and the lowest unoccupied molecular orbital (LUMO) is at the special point X $(\frac{1}{2},0,0)$. The indirect band gaps of $Cs_2Bi_2ZnS_5$ and $Cs_2Bi_2CdS_5$ are 1.85 and 1.75 eV, respectively. The latter value is in surprisingly good agreement with experiment.

In order to understand the distribution of the valence orbitals of each atom near the Fermi level, the density of states (DOS) of these two compounds were calculated.

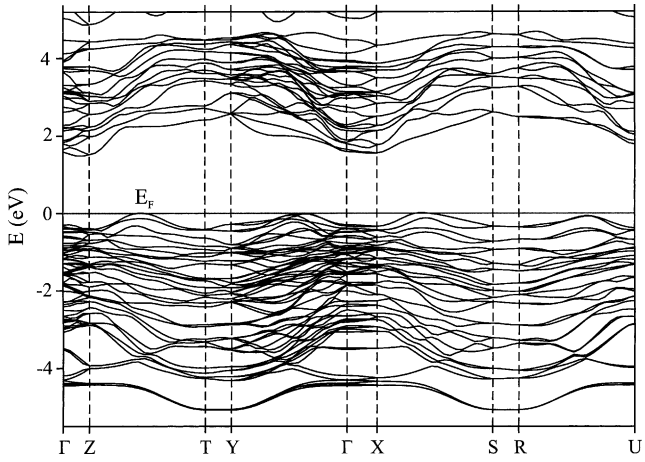

Fig. 6. The band structure of $Cs_2Bi_2ZnS_5$, and the special k-points are Γ (0, 0, 0), X $(\frac{1}{2},0,0)$, Y $(0,\frac{1}{2},0)$, Z $(0,0,\frac{1}{2})$, R $(\frac{1}{2},\frac{1}{2},\frac{1}{2})$, S $(\frac{1}{2},\frac{1}{2},0)$, T $(0,\frac{1}{2},\frac{1}{2})$, and U $(\frac{1}{2},0,\frac{1}{2})$.

Again take $Cs_2Bi_2ZnS_5$ as the example. The total and partial DOS are displayed in Fig. 7. The orbitals of S (3*s* and 3*p*), Zn (3*d* and 4*s*), and Bi (6*s* and 6*p*) dominate the states in the energy range from −15 to 5 eV. The states of S(3*s*), Zn (3*d*), and Bi (6*s*) are below the Fermi level, and there are some contributions from the remaining states, mainly from S (3*p*), Bi (6*p*), and Zn (4*s*), and slightly from Zn (4*p*). The region −15 to −8 eV is composed of S (3*s*) and Bi (6*s*) states; the region with very sharp peaks near −7 eV belongs to the highly localized Zn (3*d*) states; the region from −7 to 0 eV is dominated by some states of S (3*p*), Bi (6*p*), and Zn (4*s*); and the region from 0 to 5 eV consists of some states of S (3*p*), Bi (6*p*), and Zn (4*s*). The entire energy region from −15 to 5 eV can be divided into two parts: the region from −15 to −7 eV can be considered that of core states, and the other that of valence states. The orbitals of S(3*s*), Zn (3*d*), and Bi (6*s*) are occupied, as we would expect from the classic model of Cs^+ ($6s^0$), Bi^{3+} ($6s^26p^0$), Zn^{2+} ($3d^{10}4s^04p^0$), and S^{2-} ($3s^23p^6$). But the calculations (Fig. 7) indicate that the empty orbitals of Bi (6*p*) and Zn (4*s* and 4*p*) interact with the occupied S (3*p*) orbitals leading to some bonding overlap between the Bi/Zn and S atoms, and that some states of Bi (6*p*) and Zn (4*s* and 4*p*) are filled whereas some states of S (3*p*) are unoccupied. The S (3*p*) orbital is mainly responsible for the HOMO, and the Bi (6*p*) and S (3*p*) orbitals for the LUMO. Thus, the valence bands (Fig. 6) are constructed mainly from S (3*p*) and Bi (6*p*) states in this energy region from −5 to 5 eV. The optical transitions of $Cs_2Bi_2ZnS_5$ and $Cs_2Bi_2CdS_5$ should be mainly between these orbitals with *p*-character.

The crystal orbital Hamiltonian populations (COHP) were calculated for the bonds Bi1–S3 (3.211(2) Å) and Bi1–S4 (2.608(2) Å), respectively. The plots of –COHP versus energy for these two bonds are displayed in

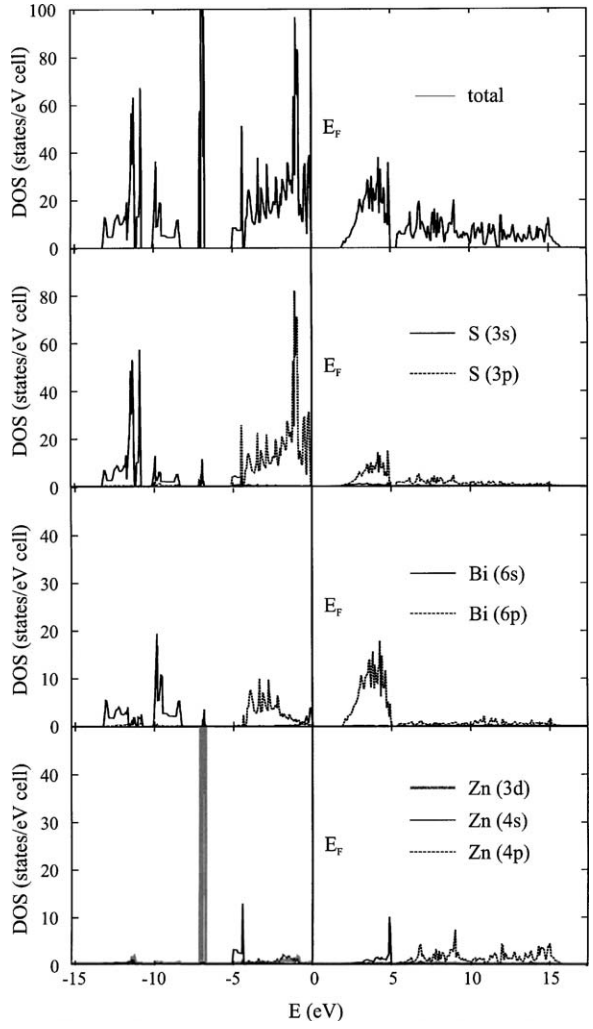

Fig. 7. The total and partial (Bi, Zn, S) density of states (DOS) of $Cs_2Bi_2ZnS_5$.

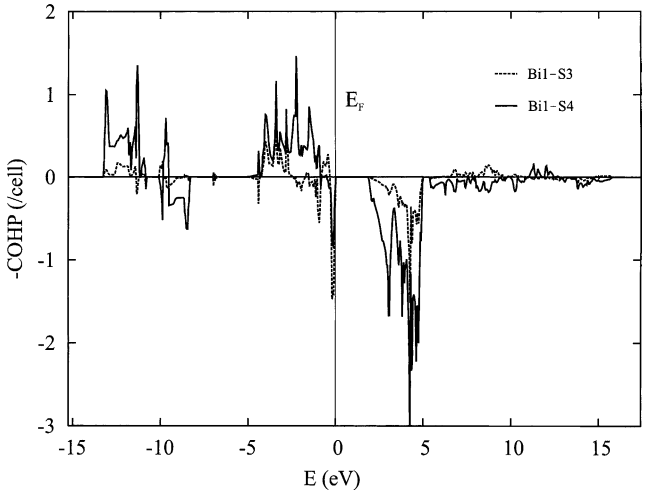

Fig. 8. The crystal orbital Hamiltonian populations (–COHP) (a) between Bi1–S3 and (b) between Bi1–S4, respectively, in $Cs_2Bi_2ZnS_5$.

Fig. 8. Negative, zero, and positive –COHP values represent bonding, nonbonding, and antibonding interactions, respectively, and the absolute value reflects the intensity of the interaction. The value of –COHP of Bi1–S3 and the integration of the –COHP values up to Fermi level are both small, consistent with the long and hence more ionic bond. The values of –COHP and the integration are significantly larger for the Bi1–S4 bond, indicating much stronger covalent bonding.

Acknowledgments

This research was supported by NSF Grant DMR00-96676. Use was made of the Central Facilities supported by the MRSEC program of the National Science Foundation (DMR00-76097) at the Materials Research Center of Northwestern University. We thank Kwasi Mitchell for his assistance.

References

[1] W.M. Yim, F.D. Rosi, Solid-State Electron. 15 (1972) 1121–1140.
[2] D.-Y. Chung, T. Hogan, P. Brazis, M. Rocci-Lane, C. Kannewurf, M. Bastea, C. Uher, M.G. Kanatzidis, Science 287 (2000) 1024–1027.
[3] T.M. Tritt, M.G. Kanatzidis, H.B. Lyon Jr., G.D. Mahan, Thermoelectric Materials-New Directions and Approaches, Vol. 478, Materials Research Society, Pittsburgh, PA, 1997.
[4] B. Eisenmann, R. Zagler, Z. Kristallogr. 197 (1991) 257–258.
[5] H.A. Harwig, A.G. Gerards, J. Solid State Chem. 26 (1978) 265–274.
[6] T. Takahashi, H. Iwahara, Mater. Res. Bull. 13 (1978) 1447–1453.
[7] P. Schmidt, O. Rademacher, H. Oppermann, Z. Anorg. Allg. Chem. 625 (1999) 255–261.
[8] B. Eisenmann, H. Schäfer, Z. Anorg. Allg. Chem. 456 (1979) 87–94.
[9] M.G. Kanatzidis, T.J. McCarthy, T.A. Tanzer, L.-H. Chen, L. Iordanidis, T. Hogan, C.R. Kannewurf, C. Uher, B. Chen, Chem. Mater. 8 (1996) 1465–1474.
[10] T.J. McCarthy, S.-P. Ngeyi, J.-H. Liao, D.C. DeGroot, T. Hogan, C.R. Kannewurf, M.G. Kanatzidis, Chem. Mater. 5 (1993) 331–340.
[11] D. Schmitz, W. Bronger, Z. Naturforsch B: Anorg. Chem. Org. Chem. 29 (1974) 438–439.
[12] O. Glemser, M. Filcek, Z. Anorg. Allg. Chem. 279 (1955) 321–323.
[13] D.-Y. Chung, K.-S. Choi, L. Iordanidis, J.L. Schindler, P.W. Brazis, C.R. Kannewurf, B. Chen, S. Hu, C. Uher, M.G. Kanatzidis, Chem. Mater. 9 (1997) 3060–3071.
[14] M. Ohmasa, W. Nowacki, Z. Kristallogr. 137 (1973) 422–432.
[15] V. Kocman, E.W. Nuffield, Acta Crystallogr B: Struct. Crystallogr. Cryst. Chem. 29 (1973) 2528–2535.
[16] J.C. Portheine, W. Nowacki, Z. Kristallogr. 141 (1975) 387–402.
[17] I. Kohatsu, B.J. Wuensch, Acta Crystallogr B: Struct. Crystallogr. Cryst. Chem. 27 (1971) 1245–1252.
[18] M. Ohmasa, W. Nowacki, Z. Kristallogr, Kristallgeom. Kristallphys. Kristallchem. 132 (1970) 71–86.
[19] I. Kohatsu, B.J. Wuensch, Z. Kristallogr, Kristallgeom. Kristallphys. Kristallchem. 138 (1973) 343–365.
[20] W.G. Mumme, Am. Mineral. 60 (1975) 300–308.
[21] H. Horiuchi, B.J. Wuensch, Can. Mineral. 14 (1976) 536–539.
[22] H. Horiuchi, B.J. Wuensch, Can. Mineral. 15 (1977) 527–535.
[23] D. Topa, E. Makovicky, T. Balic-Zunic, P. Berlepsch, Eur. J. Mineral. 12 (2000) 825–833.

[24] Y. Yang, P. Brazis, C.R. Kannewurf, J.A. Ibers, J. Solid State Chem. 155 (2000) 243–249.
[25] F.Q. Huang, K. Mitchell, J.A. Ibers, J. Alloys Compd. 325 (2001) 84–90.
[26] J. Yao, B. Deng, D.E. Ellis, J.A. Ibers, J. Solid State Chem. 41 (2002) 7094–7099.
[27] I. Kohatsu, B.J. Wuensch, Acta Crystallogr. B: Struct. Crystallogr. Cryst. Chem. 32 (1976) 2401–2409.
[28] S.A. Sunshine, D. Kang, J.A. Ibers, J. Am. Chem. Soc. 109 (1987) 6202–6204.
[29] Bruker, SMART Version 5.054 Data Collection and SAINT-Plus Version 6.22 Data Processing Software for the SMART System, 2000. Bruker Analytical X-ray Instruments, Inc., Madison, WI, USA.
[30] G.M. Sheldrick, SHELXTL DOS/Windows/NT Version 6.12, 2000. Bruker Analytical X-ray Instruments, Inc., Madison, WI, USA.
[31] L. Hedin, B.I. Lundqvist, J. Phys. Chem. Solids 4 (1971) 2064–2083.
[32] O.K. Andersen, Phys. Rev. B 12 (1975) 3060–3083.
[33] O.K. Andersen, O. Jepsen, Phys. Rev. Lett. 53 (1984) 2571–2574.
[34] O. Jepsen, O.K. Andersen, Z. Phys. B 97 (1995) 35–47.
[35] W.R.L. Lambrecht, O.K. Andersen, Phys. Rev. B 34 (1986) 2439–2449.
[36] O. Jepsen, O.K. Andersen, Solid State Commun. 9 (1971) 1763–1767.
[37] P.-O. Löwdin, J. Chem. Phys. 19 (1951) 1396–1401.
[38] R. Dronskowski, P.E. Blöchl, J. Phys. Chem. 97 (1993) 8617–8624.
[39] C.J. Bradley, A.P. Cracknell, The Mathematical Theory of Symmetry in Solids. Representation theory for point groups and space groups, Clarendon Press, Oxford, 1972.
[40] W.G. Mumme, J.A. Watts, Acta Crystallogr. B: Struct. Crystallogr. Cryst. Chem. 36 (1980) 1300–1304.
[41] T. Srikrishnan, W. Nowacki, Z. Kristallogr. 141 (1975) 174–192.
[42] K.O. Klepp, J. Alloys Compd. 182 (1992) 281–288.
[43] K.O. Klepp, K. Prager, Z. Naturforsch. B: Anorg. Chem. Org. Chem. 47 (1992) 491–496.
[44] M.G. Kanatzidis, Y. Park, Chem. Mater. 2 (1990) 99–101.
[45] R.M.H. Banda, D. Craig, I.G. Dance, M. Scudder, Polyhedron 10 (1) (1991) 41–45.
[46] N.N. Greenwood, A. Earnshaw, Chemistry of the Elements, Pergamon Press, New York, 1989.
[47] M. Wakeshima, Y. Hinatsu, J. Solid State Chem. 159 (2001) 163–169.
[48] Y. Yang, J.A. Ibers, J. Solid State Chem. 149 (2000) 384–390.
[49] M.F. Mansuetto, P.M. Keane, J.A. Ibers, J. Solid State Chem. 105 (1993) 580–587.
[50] M.F. Mansuetto, P.M. Keane, J.A. Ibers, J. Solid State Chem. 101 (1992) 257–264.
[51] M.A. Pell, J.A. Ibers, J. Alloys Compd. 240 (1996) 37–41.
[52] M.F. Mansuetto, J.A. Ibers, J. Solid State Chem. 117 (1995) 30–33.